Title

Mapping Abnormal Subcortical Brain Morphometry in an Elderly HIV+ Cohort



Authors

Wade, Benjamin SC

Valcour, Victor G

Wendelken-Riegelhaupt, Lauren

et al.

Publication Date

2015-04-01

DOI

10.1109/isbi.2015.7164033

Peer reviewed

HHS Public Access

Author manuscript

*Proc IEEE Int Symp Biomed Imaging*. Author manuscript; available in PMC 2016 April 01.

Published in final edited form as:

*Proc IEEE Int Symp Biomed Imaging*. 2015 April ; 2015: 971–975. doi:10.1109/ISBI.2015.7164033.

# MAPPING ABNORMAL SUBCORTICAL BRAIN MORPHOMETRY IN AN ELDERLY HIV+ COHORT

**Benjamin S.C. Wade**[1], **Victor G. Valcour**[2], **Lauren Wendelken-Riegelhaupt**[2], **Pardis Esmaeili-Firidouni**[2], **Shantanu H. Joshi**[4], **Yalin Wang**[5], and **Paul M. Thompson**[1]

[1]Imaging Genetics Center, University of Southern California, Los Angeles, CA, USA

[2]Memory and Aging Center, Dept. of Neurology, University of California, San Francisco, CA, USA

[3]Taub Institute for Research on Alzheimer's Disease and the Aging Brain, Columbia University Medical Center, New York, NY, USA

[4]Ahmanson-Lovelace Brain Mapping Center, Department of Neurology, UCLA, CA, USA

[5]School of Computing, Informatics, and Decision Systems Engineering, Arizona State University, Tempe, AZ, USA

## Abstract

Over 50% of HIV+ individuals exhibit neurocognitive impairment and subcortical atrophy, but the pattern of brain abnormalities associated with HIV is still poorly understood. Using parametric surface-based shape analyses, we mapped the 3D profile of subcortical morphometry in 63 HIV+ participants and 31 uninfected controls.

The thalamus, corpus striatum, hippocampus, amygdala, brainstem, callosum and ventricles were segmented from brain MRIs. To investigate subcortical shape, we analyzed the Jacobian determinant (JD) and radial distances (RD) for structure surfaces. We also investigated effects of nadir CD4+ T-cell counts, viral load, and illness duration on subcortical morphology.

Our results characterize subcortical morphometry in older HIV+ people, where participants showed significant volumetric enlargements in the thalamus, left pallidum and the ventricles while showing a reduction in the callosum. Further, RD maps revealed atrophy of the left thalamus and expansion of the brainstem in HIV. RD and JD maps of the right pallidum identified tissue expansion associated with illness duration while the left pallidum showed anterior atrophy and posterior expansion associated with viral load.

### Index Terms

HIV; subcortical; shape analysis; MRI; random forest; classification; regularization

## 1. INTRODUCTION

Combined antiretroviral therapy (cART) has vastly improved the quality of life for many people infected with HIV, allowing many to live to an advanced age. Yet even among those receiving long-term cART, around 50% develop HIV-associated neurocognitive disorders

(HAND) [1, 2]. HAND is characterized by several and psychomotor and cognitive impairments in working memory, processing speed, executive function and attention [3–5].

The cognitive profile of HAND is thought to result from neuronal atrophy in the CNS due to neurotoxic effects of HIV. Several brain regions may show atrophy, including the frontal cortices, periventricular white matter, basal ganglia and other subcortical regions [6]. The extent of psychomotor dysfunction in HIV has been associated with basal ganglia atrophy [7]. Different patterns of basal ganglia atrophy have been reported to accompany HAND including both volumetric increases (hypertrophy) [8] and reductions hypotrophy [9]. As suggested by Hua et al. [10], these divergent reports may be due in part to the stage of HIV infection assessed.

Subcortical brain regions have been implicated in HAND, but the exact profile of HIV-associated brain abnormalities is poorly understood. More sensitive biomarkers for detection of HAND may help clinicians identify which HIV+ subjects are prone to developing neurocognitive disorders, and to receive early intervention. An important step in the characterization of the HIV neurophenotype is to describe local differences in morphometry that accompany the illness. Beyond global volumetric measures of abnormalities, surface-based shape descriptors can better localize tissue atrophy or expansion.

Here we report on both the subcortical volumetric and 3D surface-based shape abnormalities in a cohort of 63 elderly HIV+ subjects scanned with structural magnetic resonance imaging (MRI) as part of the UCSF HIV Over 60 Cohort study. To study subcortical shape, we analyzed: (1) the Jacobian determinant (JD) indexed over structures' surface coordinates and (2) radial distances (RD) of structure surfaces from a medial curve. JD maps of a subcortical surface indicate localized atrophy where the determinant is less than 1, and expansion in regions where the JD is greater than 1 [11]. Complementary to JD, the RD indicates the local "thickness" of the structure.

We additionally tested associations of morphological descriptors with several common HIV clinical indices: nadir CD4+ (nCD4) T-cell count, illness duration, and HIV RNA concentration. We hypothesized that subcortical shape analysis would reveal regions of significant atrophy in HIV+ people relative to matched controls and in relation to clinical markers of HIV-related disease.

The diagnostic classification performance of each of the three descriptors was then assessed, via a two-fold cross validation using a guided regularized random forest (RF) classifier [12]. Developed by Breiman [13], the RF machine learning algorithm is a computationally efficient classification method used in a wide array of fields including microarray analysis [14] and computer vision [15].

## 2. MATERIAL AND METHODS

### 2.1. Subjects

A sample of 63 elderly HIV+ subjects (4 female; age=65.35 ± 2.21) and 31 uninfected elderly controls (2 female; age=64.68 ± 4.57) were recruited as part of a San Francisco Bay

Area study of elderly people with HIV. HIV+ participants had an average nCD4 count of 204.96 ± 154.85 cells/$mm^3$, an average illness duration of 20.39 years ± 6.31 years. 24 HIV + participants had detectable concentrations of viral RNA above 50 copies/$mm^3$. Among those with detectable HIV RNA, the average viral load was 16,400 ± 76,400 copies/$mm^3$. All subjects gave informed consent to take part in the study.

### 2.2. Image acquisition and segmentation

Each subject underwent a whole-brain magnetic resonance imaging (MRI) anatomical brain scan on a Siemens 3 Tesla TIM Trio scanner with a 12-channel head coil. T1-weighted MP-RAGE sequences (240 × 256 matrix; FOV = 256mm; 160 slices; voxel size = 1.0 × 1.0 × 1.0 $mm^3$; TI = 900 ms; TR = 2300 ms; TE = 2.98 ms; flip angle = 9°.

FreeSurfer [16] was used to segment the thalamus, caudate, putamen, pallidum, hippocampus, amygdala, accumbens, brain stem, callosum and lateral and third ventricular spaces from the raw MRIs. All segmentations underwent visually inspection for quality control.

### 2.3. Morphological descriptors

The volume of each VOI was computed using FreeSurfer. Each binary image resulting from the segmentation was converted into a parametric 3D mesh model. Each mesh was obtained using the marching cubes algorithm [17]. A two-step smoothing procedure was applied to each mesh consisting of mesh simplification using progressive meshes [18] along with mesh refinement using Loop subdivision surface [19]. The JD was locally computed at each vertex on the mesh and approximated by the determinant of the derivative map of the local parameterization induced by a conformal mapping. The conformal mapping itself was constructed based on a holomorphic 1-form as described in Wang et al. [11]. A determinant value of greater than 1 denotes tissue expansion, whereas a value of less than 1 denotes tissue atrophy locally on the surface.

The RD of the surface mesh is calculated by first computing a 3D medial core which traverses the volume's local center. The radial distance from each vertex to the nearest point of the medial core provides the index of radial distance, a proxy for the structure's local thickness [20, 21].

### 2.4. Statistical methods

Multiple linear regression was used to model influences of HIV status, nCD4 count, viral load and illness duration on each surfaces' morphometry. The general linear model assumed the following form,

$$outcome = \beta_0 + \beta_1 \cdot Main\ Effect + \beta_2 \cdot Age + \beta_3 \cdot Sex + \beta_4 + Instracranial\ volume + \varepsilon. \quad \text{Eq. (1)}$$

Here the outcome measure is global volume, the local JD or RD - and the Main Effect is one of HIV status, nCD4 count, viral load or illness duration. This model was fit at each of 15,000 vertices comprising each surface when the outcome of interest was the JD or RD. HIV status and viral load were each modeled dichotomously; HIV status was coded as

positive or negative and viral load as detectable (above 50 viral RNA copies/mm$^3$) or undetectable (i.e. binary). nCD4 and illness duration were modeled continuously.

We controlled for multiple comparisons using the standard false discovery rate (FDR) method with a falsepositive rate of 5% ($q$ = 0.05) [22]. FDR was performed separately for volumetric and shape-based tests. For the family of volumetric tests, FDR was applied to the set of all subcortical structures. For shape analyses we applied an FDR correction within the family of all tests performed on a single surface; correcting for 15,000 separate tests on each surface. As a *post hoc* analysis we report the tests that survived FDR correction over all vertices from each surface.

### 2.5. Feature selection and classification

Because each mesh was composed of 15,000 vertices having RD and JD as an attribute we performed feature selection to reduce the risk of overfitting our training data in the cross validation process. Recently, a combined feature selection and classification algorithm called guided regularized random forests (GRRF) [23] was proposed to handle high-dimensional feature spaces within a RF framework. GRRF uses importance scores from each variable obtained using a standard RF to inform the penalty terms in a regularized RF's feature selection process. GRRF selected features are submitted to a standard RF to classify the groups. GRRF is detailed in [23, 24]; its steps are summarized below.

**2.5.1. Random forests and importance scores—**RFs are supervised classifiers composed of an ensemble of classification and regression trees (CART) [13], and use the majority vote of its terminal nodes to predict the class of a given observation. RF CARTs are constructed from a bootstrapped sample of observations with approximately 1/3$^{rd}$ left out. At each node of the CART a random subset of $\sqrt{M}$ features is selected and the Gini index is calculated for each feature at the given node, v. Gini(v) is given by:

$$Gini(v)=\sum_{C=1}^{C}\hat{p}_c^v(1-\hat{p}_c^v), \quad \text{Eq. (2)}$$

where $\hat{p}_c^v$ is the proportion of observations belonging to class C at node v. The objective of the RF algorithm is to split each CART node by the feature $X_i$ which maximizes the class purity of the resultant child nodes, $v^r$ and $v^l$. This is done by choosing the maximum *Gain* ($X_i$, $v$) given by,

$$Gain(X_i,v)=\ Gini(X_i,v)-\omega_l Gini(X_i,v^l)-\omega_r Gini(X_i,v^r), \quad \text{Eq. (3)}$$

where $\omega_l$ and $\omega_r$ are the proportions of observations in node v assigned to child nodes $v^r$ and $v^l$, respectively. The importance I, of feature $X_i$ is given by the summation of the decreases in the Gini index at each node where the CART was partitioned by $X_i$ [25]. That is,

$$I_{X_i}=\frac{1}{total\ tree\ number}\sum_{v\in S_{X_i}} Gain(X_i,v), \quad \text{Eq. (4)}$$

where $S_{X_i}$ indicates the set of all nodes split by $X_i$. The CARTs were used in their full unpruned form.

**2.5.2. Guided regularized random forests—**GRRFs are an extension of RFs that use normalized importance scores, $I_n$, from an ordinary RF to parameterize the regularization of $Gain\ (X_i, v)$ in a second RF. This allows GRRF to apply a separate penalty to each feature,

$$Gain_{reg}(X_i, v) = \begin{cases} \lambda_i Gain(X_i, v) & X_i \notin \mathrm{F} \\ Gain(X_i, v) & X_i \in \mathrm{F} \end{cases}, \quad \text{Eq. (5)}$$

where F is the set of features used to split previous nodes in previous trees and $\lambda_i$ is the regularization coefficient for feature $X_i$ given by,

$$\lambda_i = (1-\gamma) + \gamma I_{n_i}, \quad \text{Eq. (6)}$$

where $\gamma \in [0, 1]$, is a constant argument to GRRF to control the degree of penalization.

GRRF feature selection was applied to the RD and JD maps of each VOI separately. The selected shape-based features from each VOI were combined and used as input into a final RF classifier. We report the classification accuracies of three separate RF classifiers constructed from the (1) volume of each structure, (2) RD, and (3) JD maps of each structure. Each GRRF and subsequent RF was composed of 3,000 decision trees. We set the base penalization coefficient, $\gamma$, to 0.5. 2-fold cross validation was performed by constructing each RF based on a training set of 32 HIV+ and 16 HIV- subjects; the HIV status of the remaining subjects was then predicted by the model fitted using the training data.

## 3. RESULTS

Several associations were revealed between subcortical morphometry and HIV status and clinical parameters.

### 3.1. HIV status

Volumetrically, the callosum ($\beta_{dx} = -290$, $t = -2.81$, $p < 0.05$), left pallidum ($\beta_{dx} = -180$, $t = -3.47$, $p < 0.01$), left putamen ($\beta_{dx} = -330$, $t = -2.40$, $p < 0.05$), left thalamus ($\beta_{dx} = -390$, $t = -2.91$, $p < 0.05$) and right thalamus ($\beta_{dx} = -440$, $t = -3.00$, $p < 0.05$) were all significantly smaller in HIV+ participants. Ventricular spaces were, on average, enlarged in HIV+ subjects. The left lateral ($\beta_{dx} = 5100$, $t = 2.88$, $p < 0.05$), right lateral ($\beta_{dx} = 3900$, $t = 2.41$, $p < 0.05$) and third ($\beta_{dx} = 420$, $t = 3.68$, $p < 0.01$) ventricular spaces were all significantly larger in HIV+ participants.

In the shape domain, RD maps revealed a significantly enlarged central region of the brain stem; an area corresponding to the location of the cerebral aqueduct and fourth ventricle. The RD of the left-hemisphere thalamic surface was significantly decreased in its anterior aspect (Figure 1a).

### 3.2. Nadir CD4+ counts

There were no detectable volumetric or shape-based associations between nCD4 counts and morphometry.

### 3.3. Viral load

No significant volumetric differences were found between HIV+ participants with and without detectable viral RNA levels. Significant shape-based differences were observed in the left pallidum. Both RD and JD maps of the left pallidum suggest a different pattern of morphometry associated with viral load. The anterior aspect of the left putamen exhibits atrophy while the posterior portion expands in subjects with detectable viral RNA. Figures 1b–c show the RD and JD maps respectively.

### 3.4. HIV duration

The volume of the right pallidum ($\beta_{duration}$= 6.3, t = 2.43, p > 0.05) was positively associated with illness duration prior to correction for multiple comparisons but failed to survive FDR. Corroborating this, both RD and JD maps of the right pallidum indicate significant local expansion in its central aspect in relation to increased illness duration; RD and JD results survived FDR (Figure 1d–e).

### 3.5. Classification performance

GRRF-RF classification of HIV+ versus HIV- people using only volumetric information yielded an area under the receiver operating characteristic (ROC) curve (AUC) of 66.9% (95% CI [48.94, 84.85]). RD features alone provided an AUC of 53.79% (95% CI [33.31, 74.28]) while the AUC for JD features was 74.71% (95% CI [58.89, 90.54]).

We used DeLong's test for two correlated ROC curves [26] to compare the various AUCs in a statistical framework. Prior to FDR, the AUC of the JD maps (DeLong's Z = 2.05, p > 0.05) was larger (better) than the RD AUC, but the difference did not survive FDR.

## 4. DISCUSSION

Compared to other prevalent forms of dementia, relatively little is known about brain differences in people with HIV or HAND. It is critical to characterize how HIV may affect various brain regions as well as develop biomarkers to track the extent of its effects in the central nervous system. Using standard volumetric and novel surface-based shape descriptors we were able to identify several important HIV-related patterns of brain abnormalities. Associations were also found between surface-based morphometry and clinical parameters commonly measured in HIV+ patients receiving treatment.

We correctly predicted that HIV positivity and more extreme (poorer) clinical measures would be associated with greater subcortical atrophy, but we also observed unexpected effects. Surprisingly, the bilateral pallida was shown to be enlarged in association with poorer clinical scores; the right with longer illness duration and the left posteriorly with detectable viral RNA concentrations.

As this is specifically an elderly cohort of HIV+ participants, many of whom survived infection prior to the advent of modern cART, it is possible that some of these observed differences may be the result of a survivor bias in our sample.

Volumetric and shape descriptors characterize different aspects of brain abnormalities in HIV. Volumetric measures identified a large set of structures differing in size between diagnostic groups, but shape measures alone were able to detect the more subtle associations between clinical measures and subcortical morphometry. This is the first study that combines both shape and volumetric descriptors in a classification framework for characterizing HIV related brain abnormalities in patients.

## Acknowledgments

This work was supported in part by NIH 'Big Data to Knowledge' (BD2K) Center of Excellence grant U54 EB020403, funded by a cross-NIH consortium including NIBIB and NCI and by the National Science Foundation Graduate Research Fellowship under Grant No. DGE-0707424.

## REFERENCES

1. Cysique L, Maruff P, Brew B. Prevalence and pattern of neuropsychological impairment in human immunodeficiency virus-infected/acquired immunodeficiency syndrome (HIV/AIDS) patients across pre- and post-highly active antiretroviral therapy eras: A combined study of two cohorts. Journal of Neurovirology. 2004; 10:350–357. [PubMed: 15765806]
2. Simioni S, Cavassini M, Annoni JM, Rimbault Abraham A, Bourquin I, Schiffer V, et al. Cognitive dysfunction in HIV patients despite long-standing suppression of viremia. AIDS. 2010; 24:1243–1250. [PubMed: 19996937]
3. Brew BJ. Evidence for a change in AIDS dementia complex in the era of highly active antiretroviral therapy and the possibility of new forms of AIDS dementia complex. Aids. 2004; 18:75–78. [PubMed: 15090832]
4. Heaton RK GI, Butters N, White DA, Kirson D, Atkinson JH. The HNRC 500-Neuropsychology of HIV infection at different disease stages. J. International Neuropsychological Society. 1995; 1:231–251.
5. Sacktor N, McDermott M, Marder K, Schifitto G, Selnes O, McArthur J, et al. HIV-associated cognitive impairment before and after the advent of combination therapy. Journal of NeuroVirology. 2002; 8:136–142. [PubMed: 11935465]
6. Wiley CA, Achim CL, Christopherson C, Kidane Y, Kwok S, Masliah E, et al. HIV mediates a productive infection of the brain. Aids. 1999; 13:2055–2059. [PubMed: 10546857]
7. Küper M, Rabe K, Esser S, Gizewski ER, Husstedt IW, Maschke M, et al. Structural gray and white matter changes in patients with HIV. Journal of Neurology. 2011; 258:1066–1075. [PubMed: 21207051]
8. Castelo J, Courtney MG, Melrose RJ, Stern CE. Putamen hypertrophy in nondemented patients with human immunodeficiency virus infection and cognitive compromise. Archives of Neurology. 2007; 64:1275–1280. [PubMed: 17846265]
9. Jernigan TL, Gamst AC, Archibald SL, Fennema-Notestine C, Mindt MR, Marcotte TL, et al. Effects of Methamphetamine Dependence and HIV Infection on Cerebral Morphology. American Journal of Psychiatry. 2005; 162:1461–1472. [PubMed: 16055767]
10. Hua X, Boyle CP, Harezlak J, Tate DF, Yiannoutsos CT, Cohen R, et al. Disrupted cerebral metabolite levels and lower nadir CD4 + counts are linked to brain volume deficits in 210 HIV-infected patients on stable treatment. NeuroImage. Clinical. 2013; 3:132–142. [PubMed: 24179857]
11. Wang Y, Yuan L, Shi J, Greve A, Ye J, Toga AW, et al. Applying tensor-based morphometry to parametric surfaces can improve MRI-based disease diagnosis. NeuroImage. 2013; 74:209–230. [PubMed: 23435208]
12. Houtao D, George R. Gene selection with guided regularized random forest. Pattern Recogn. 2013; 46:3483–3489.
13. Breiman L. Random Forests. Machine Learning. 2001; 45:5–32.

14. Geurts P, Fillet M, de Seny D, Meuwis M-A, Malaise M, Merville M-P, et al. Proteomic mass spectra classification using decision tree based ensemble methods. Bioinformatics. 2005 Jul 15.21:3138–3145. 2005. [PubMed: 15890743]
15. Shotton, J.; Fitzgibbon, A.; Cook, M.; Sharp, T.; Finocchio, M.; Moore, R., et al. Real-Time Human Pose Recognition in Parts from Single Depth Images. In: Cipolla, R.; Battiato, S.; Farinella, GM., editors. Machine Learning for Computer Vision. Vol. 411. Berlin Heidelberg: Springer; 2013. p. 119-135.
16. Dale AM, Fischl B, Sereno MI. Cortical surface-based analysis. I. Segmentation and surface reconstruction. Neuroimage. 1999 Feb.9:179–194. [PubMed: 9931268]
17. William EL, Harvey EC. Marching cubes: A high resolution 3D surface construction algorithm. SIGGRAPH Comput. Graph. 1987; 21:163–169.
18. Hoppe, H. Progressive Meshes; Proceedings of the 23rd Annual Conference on Computer Graphics and Interactive Techniques; 1996. p. 99-108.
19. Loop CT. Smooth Subdivision Surfaces Based on Triangles. Mathematics Department, University of Utah. 1987
20. Apostolova LG, Dinov ID, Dutton RA, Hayashi KM, Toga AW, Cummings JL, et al. 3D comparison of hippocampal atrophy in amnestic mild cognitive impairment and Alzheimer's disease. Brain : a journal of neurology. 2006; 129:2867–2873. [PubMed: 17018552]
21. Apostolova LG, Morra JH, Green AE, Hwang KS, Avedissian C, Woo E, et al. Automated 3D mapping of baseline and 12-month associations between three verbal memory measures and hippocampal atrophy in 490 ADNI subjects. NeuroImage. 2010; 51:488–499. [PubMed: 20083211]
22. Benjamini Y, Hochberg Y. Controlling the false discovery rate- a practical and powerful approach to multiple testing. Journal of the Royal Statistical Society. 1995; 57:289–300.
23. Deng H, Runger G. Gene Selection with Guided Regularized Random Forests. 2013; 46:3483–3489.
24. Deng H. Guided Random Forest in the RRF Package. 2013:1–2.
25. Gray KR, Aljabar P, Heckemann RA, Hammers A, Rueckert D. Random forest-based similarity measures for multi-modal classification of Alzheimer's disease. NeuroImage. 65:167–175. [PubMed: 23041336]
26. DeLong ER, DeLong DM, Clarke-Pearson DL. Comparing the Areas under Two or More Correlated Receiver Operating Characteristic Curves: A Nonparametric Approach. Biometrics. 1988; 44:837–845. [PubMed: 3203132]

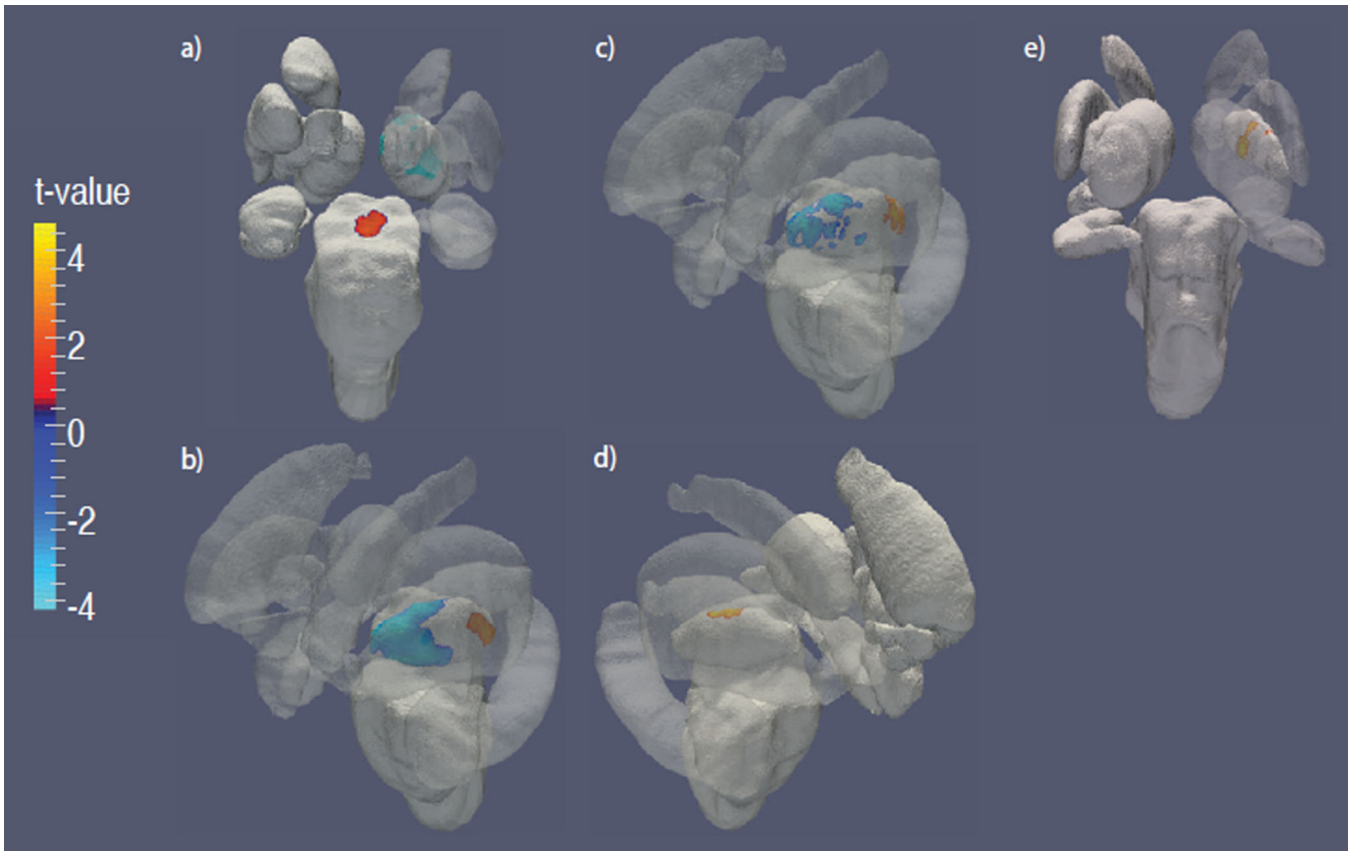


**Figure 1.**

Thresholded *t*-value maps of subcortical surfaces with significant clinical associations: (a) HIV status, (b–c) viral load and (d–e) HIV duration. RD and JD maps are thresholded to display t-values only in regions surviving FDR.

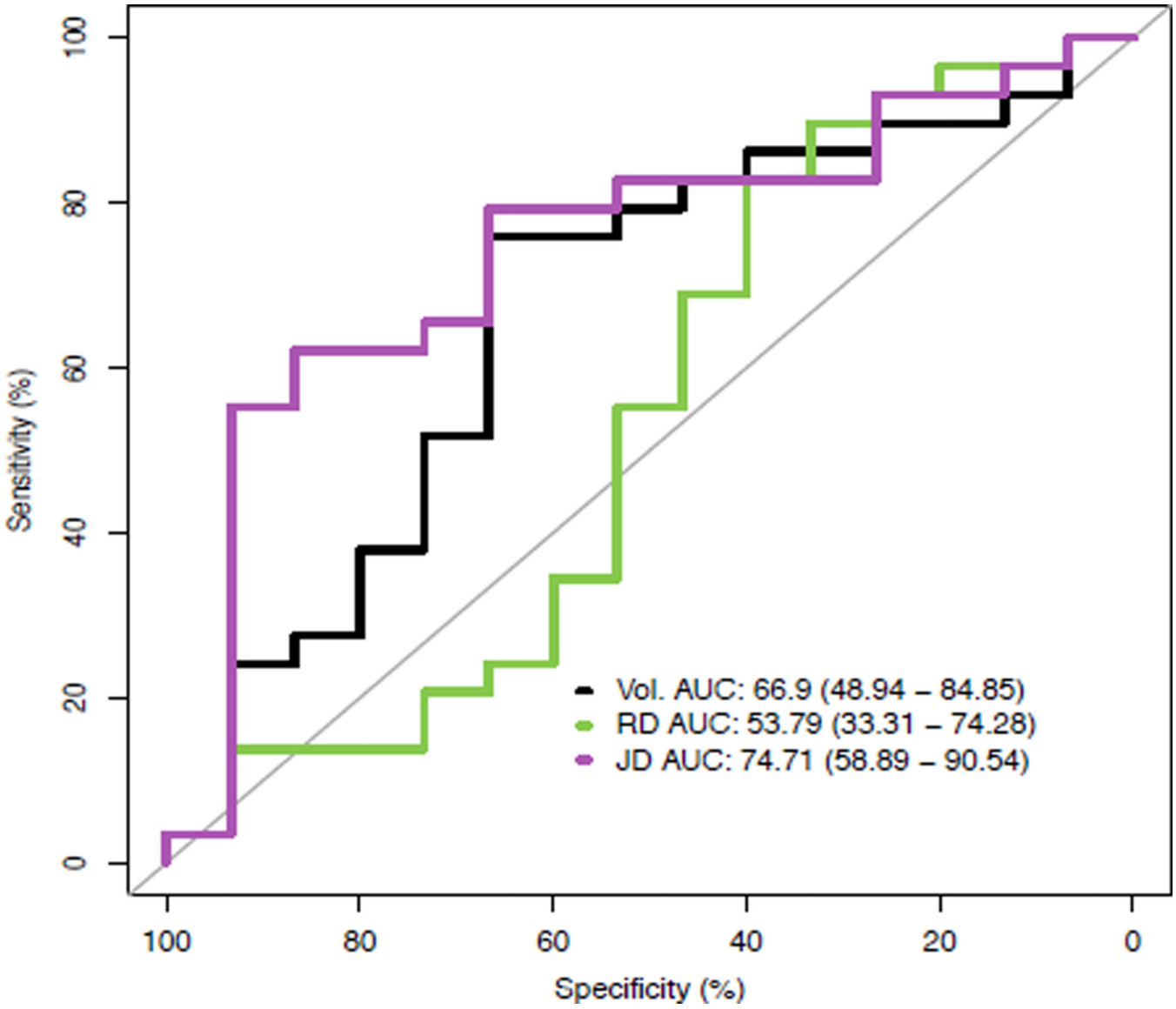


**Figure 2.**
ROC curves by morphological feature.